The Journal of Chemical Physics

Deep potential generation scheme and simulation protocol for the $Li_{10}GeP_2S_{12}$-type superionic conductors

Cite as: J. Chem. Phys. **154**, 094703 (2021); https://doi.org/10.1063/5.0041849
Submitted: 25 December 2020 • Accepted: 31 January 2021 • Published Online: 01 March 2021

Jianxing Huang, Linfeng Zhang, Han Wang, et al.

COLLECTIONS

Paper published as part of the special topic on JCP Editors' Choice 2021

This paper was selected as an Editor's Pick

View Online Export Citation CrossMark

ARTICLES YOU MAY BE INTERESTED IN

When do short-range atomistic machine-learning models fall short?
The Journal of Chemical Physics **154**, 034111 (2021); https://doi.org/10.1063/5.0031215

Machine learning for interatomic potential models
The Journal of Chemical Physics **152**, 050902 (2020); https://doi.org/10.1063/1.5126336

Perspective: Machine learning potentials for atomistic simulations
The Journal of Chemical Physics **145**, 170901 (2016); https://doi.org/10.1063/1.4966192

Lock-in Amplifiers up to 600 MHz
Zurich Instruments
Watch

AIP Publishing

© 2021 Author(s).

The Journal of Chemical Physics ARTICLE scitation.org/journal/jcp

Deep potential generation scheme and simulation protocol for the $Li_{10}GeP_2S_{12}$-type superionic conductors

Cite as: J. Chem. Phys. 154, 094703 (2021); doi: 10.1063/5.0041849
Submitted: 25 December 2020 • Accepted: 31 January 2021 •
Published Online: 1 March 2021

View Online Export Citation CrossMark

Jianxing Huang,[1] Linfeng Zhang,[2] Han Wang,[3] Jinbao Zhao,[1,a)] Jun Cheng,[1,b)] and Weinan E[2,4,c)]

AFFILIATIONS

[1]State Key Laboratory of Physical Chemistry of Solid Surfaces, iChEM, College of Chemistry and Chemical Engineering, Xiamen University, Xiamen 361005, China
[2]Program in Applied and Computational Mathematics, Princeton University, Princeton, New Jersey 08544, USA
[3]Laboratory of Computational Physics, Institute of Applied Physics and Computational Mathematics, Fenghao East Road 2, Beijing 100094, People's Republic of China
[4]Department of Mathematics, Princeton University, Princeton, New Jersey 08544, USA

[a)]**Electronic mail:** jbzhao@xmu.edu.cn
[b)]**Author to whom correspondence should be addressed:** chengjun@xmu.edu.cn
[c)]**Electronic mail:** weinan@math.princeton.edu

ABSTRACT

Solid-state electrolyte materials with superior lithium ionic conductivities are vital to the next-generation Li-ion batteries. Molecular dynamics could provide atomic scale information to understand the diffusion process of Li-ion in these superionic conductor materials. Here, we implement the deep potential generator to set up an efficient protocol to automatically generate interatomic potentials for $Li_{10}GeP_2S_{12}$-type solid-state electrolyte materials ($Li_{10}GeP_2S_{12}$, $Li_{10}SiP_2S_{12}$, and $Li_{10}SnP_2S_{12}$). The reliability and accuracy of the fast interatomic potentials are validated. With the potentials, we extend the simulation of the diffusion process to a wide temperature range (300 K–1000 K) and systems with large size (~1000 atoms). Important technical aspects such as the statistical error and size effect are carefully investigated, and benchmark tests including the effect of density functional, thermal expansion, and configurational disorder are performed. The computed data that consider these factors agree well with the experimental results, and we find that the three structures show different behaviors with respect to configurational disorder. Our work paves the way for further research on computation screening of solid-state electrolyte materials.

Published under license by AIP Publishing. https://doi.org/10.1063/5.0041849

I. INTRODUCTION

All-solid-state Li-ion batteries are among the most promising candidates for the next-generation rechargeable batteries.[1–5] Desired solid-state electrolyte (SSE) materials should have high Li^+ conductivities and wide electrochemical windows. Several groups of promising candidates, with performance competitive to current commercial liquid electrolytes (e.g., $Li_{10}GeP_2S_{12}$,[6] $Li_7La_3Zr_2O_2$,[7] and $Li_7P_3S_{11}$[8]), have been reported. Due to their relevant highest ionic conductivities, the families of $Li_{10}GeP_2S_{12}$-type materials have attracted extensive studies.[6,9–11,69,75,83–86,88,89,91]

Improvement of SSE performance benefits from the fundamental understanding of the atomic-scale diffusion process. The *ab initio* molecule dynamics (AIMD) calculation[12] has been utilized to investigate the microscopic details of the diffusion processes.[9–11,13–15] The diffusion coefficients of most superionic conductors ranges from 10^{-13} m^2/s to 10^{-10} m^2/s. Unfortunately, due to its high computational cost, AIMD is typically limited to a system size of hundreds of atoms in the time scale of tens of pico-seconds. Accurate calculation of diffusion coefficients requires simulations in the time scale of nanoseconds, which is unreachable for current AIMD methods. This makes AIMD practically impossible to accurately estimate the

Published under license by AIP Publishing

diffusion coefficients of solid-state electrolyte materials at experimental conditions, i.e., at room temperature. Therefore, one often resorts to the extrapolation strategy: assuming that a single Arrhenius relationship applies to a wide temperature range (this implicitly assumes a temperature-independent diffusion mechanism), then one can predict the ionic conductivity under working conditions (–40 °C to 80 °C) by extrapolating from the high-temperature regime (>500 K) to the low-temperature regime (<500 K).

A commonly found protocol in the literature based on this assumption is to collect high-temperature diffusion coefficients (600 K–1200 K) from 100 ps to 400 ps AIMD simulations[9–11] including 100–200 atoms and extrapolate these data to obtain room-temperature ionic conductivities. However, this extrapolation strategy based on temperature will lead to deviations up to two orders of magnitude at room temperature. As demonstrated in Fig. 1(a), AIMD calculations significantly overestimate diffusion coefficients at room temperature. This issue, in particular, when applied to SSE materials, has been comprehensively discussed by He *et al.*[23]

Even more problematically, this extrapolation approach loses predictive power when the Arrhenius-type temperature dependence breaks down, which has been discussed in detail over 40 years ago.[18] Figure 1(b) shows that three types of superionic conductors give rise to different transition behaviors of the ionic conductivity with respect to the inverse of the temperature. The temperature dependence of ionic conductivities of several typical ionic conductors is depicted in Fig. 1(c). The examples of $Li_{10.05}Ge_{1.05}P_{1.95}S_{12}$ and β-Li_3PS_4 represent the failures of the extrapolation strategy in $Li_{10}GeP_2S_{12}$-like systems. The assumption behind the extrapolation

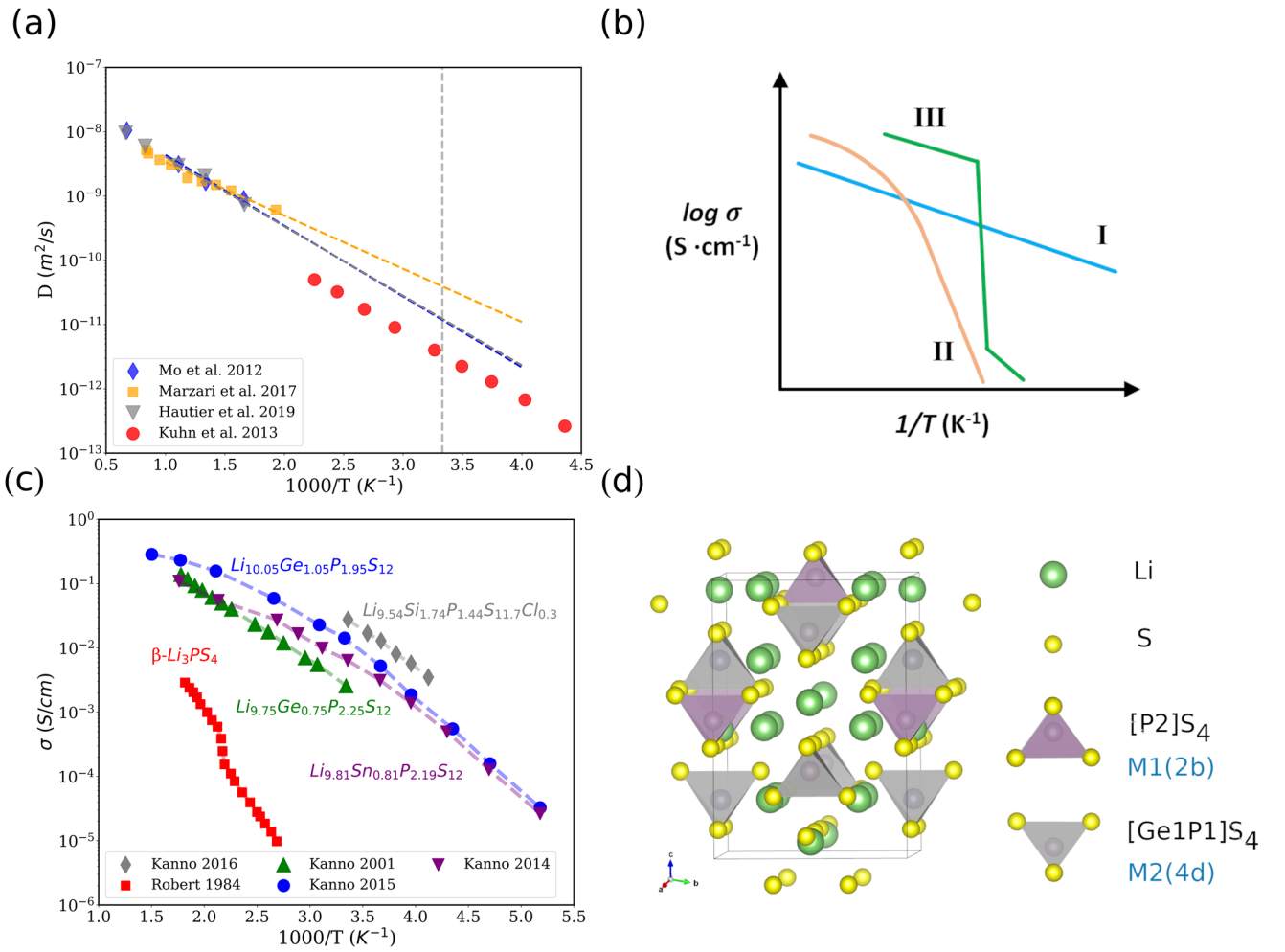

FIG. 1. (a) Diffusion coefficients of $Li_{10}GeP_2S_{12}$ by AIMD calculations[11,16] (blue, orange, and gray points) and solid state NMR measurement[17] (red points). The AIMD data are extrapolated to room temperature. The dashed vertical line corresponds to room temperature (300 K). (b) Schematic illustration of the three kinds of the temperature dependence of the conductivity, according to Ref. 18. (c) Temperature dependence of the ionic conductivity of Li-ion superionic conductors from experiments. Data were taken from β-Li_3PS_4,[19] $Li_{10.05}Ge_{1.05}P_{1.95}S_{12}$,[20] and $Li_{9.75}Ge_{0.75}P_{2.25}S_{12}$.[21] (d) Characteristics of the $Li_{10}GeP_2S_{12}$ structure. The occupation ratio of P in the M1(4d) site for all three systems is around 0.5.[6,17,22]

Published under license by AIP Publishing

strategy is only applicable to systems whose diffusion mechanisms are independent of temperature.

An explicit solution is to directly simulate the diffusion processes at room temperature, which requires larger systems and longer trajectories to ensure the convergence. Thus, acceleration of simulations without losing the accuracy of Density Functional Theory (DFT) calculation is desired. There have been ever-increasing efforts recently to develop empirical interatomic potential or model Hamiltonians involving simple analytical terms to speed up simulations for SSE materials of interest.[24–27] However, due to the relatively large errors, the empirical models are only suitable for the crude screening of materials. More recent works have utilized machine learning (ML) tools[5,28–31,73,74] to represent the many-body and nonlinear dependence of the potential energy surface (PES) on atomic positions for modeling.[32–37] In particular, applications to SSE materials, e.g., Li_3PO_4,[36] LiPON,[35] $Li_{10}GeP_2S_{12}$,[38] and Li_3N,[37] have recently been explored.

Despite these efforts, two major obstacles have remained.

First, a systematic and automatic procedure to generate uniformly accurate PES models, with a minimal set of training data, is still largely missing. The most straightforward approach is to perform extensive AIMD simulations at different temperatures and train models based on these AIMD trajectories. However, this procedure is computationally demanding, and the generated snapshots are highly correlated, reducing the quality of the training data. For this reason, a great amount of trial-and-error process is involved in most of the ML-based models, and consequently, the reliability of these models is in doubt. In addition, the performances of ML potentials depend on a few factors, including the reliability of locality assumption, quality of training data, and hyperparameters of models. Specifically, though there have been some efforts to set up ML potential generation schemes for different materials,[38–44] there lacks a well-benchmarked, automatic, and efficient scheme for the generation and validation of ML potential for Li-ion superionic conductor materials.

Second, the diffusion process is determined by the structures, e.g., lattice volume[9,11] and configurational disorder.[45–48] The structure of $Li_{10}GeP_2S_{12}$ is visualized in Fig. 1(d) in which MS_4 (M = Ge, Si, Sn, and P) tetrahedrons form the solid-like backbone and the liquid-like Li-ions are free to flow across the channels. The tetrahedral units include two groups of sites, M1(2b) and M2(4d). The M2(4d) sites could be occupied by Ge/Si/Sn/P atoms, while only P atoms are found to occupy the M1(2b) sites. The fractional occupation results in the disordered arrangement of MS_4 tetrahedral units. To the best of our knowledge, little attention has been paid to the effects of the thermal expansion of the lattice volume and configurational disorder on diffusion processes. To set up protocols to accurately compute diffusion coefficients of $Li_{10}GeP_2S_{12}$-type materials at different temperatures, technical issues of MD simulations and the effects of these factors shall be validated.

In this work, we implement a concurrent learning scheme (DP-GEN) to generate uniformly accurate Deep Potential (DP)[81,82] models for three $Li_{10}GeP_2S_{12}$-type superionic conductors ($Li_{10}GeP_2S_{12}$, $Li_{10}SiP_2S_{12}$, and $Li_{10}SnP_2S_{12}$), respectively. The reliability and performance of the DP models are examined, including the locality test, model accuracy, and speed test. With the DP models, the effects of key simulation settings, thermal expansion, and configurational disorder have been investigated. The validated protocol is applied to compute diffusion coefficients between 300 K and 1000 K. Finally, the simulation results are compared with experimental data and the differences are discussed.

II. METHODS

A. DP-GEN for $Li_{10}GeP_2S_{12}$-type structures

Using the Deep Potential Generator (DP-GEN),[49,50] a minimal set of training data is generated via an efficient and sufficient sampling process, thereby guaranteeing a reliable PES model produced by training. The flowchart of DP-GEN iteration is shown in Fig. 2. In the exploration step, model deviations are evaluated using the ensemble of trained models, and new configurations are picked according to the maximum deviation of forces (σ_f^{max}), defined as

$$\sigma_f^{max} = \max_i \sqrt{\langle \|f_i - \langle f_i \rangle\|^2 \rangle}, \tag{1}$$

where f_i is the force acting on atom i and $\langle \cdots \rangle$ denotes the average of the DP model ensemble. Configurations with small force deviations [$\sigma_f^{max} < \sigma_{low}$, yellow squares in Fig. 2(c)] are effectively covered by the training dataset with high probability. On the contrary, excessive force deviation [$\sigma_f^{max} > \sigma_{high}$, red crosses in Fig. 2(c)] implies that the configuration may diverge from the relevant physical trajectories. Therefore, none of them are picked. Only configurations whose σ_f^{max} fall between a predetermined window are labeled as *candidates* [blue circles in Fig. 2(c)]. In practice, after running several MD trajectories, the selection criterion usually produces hundreds or thousands of candidates. A small fraction of them is representative enough to improve the model, and therefore, a cutoff number (N_{label}^{max}) is set to restrict the number of candidates. These candidates are labeled and added to the original dataset for the next training. The labeling and training stages are rather standard, while there is large flexibility for the sampling strategy on how to explore the relevant configuration space in each iteration. According to Ref. 50, a practical rule of thumb is to set σ_{low} slightly larger than the training error achieved by the model and set σ_{high} 0.1 eV/Å–0.3 eV/Å higher than σ_{low}. In this paper, σ_{low} and σ_{high} are set to 0.12 eV/Å and 0.25 eV/Å, respectively.

In this work, all crystal structures are fetched from the Materials Project[51,52] database as conventional cells. The material IDs of them in the Materials Project are as follows: mp-696138 [$Li_{10}Ge(PS_6)_2$], mp-696129 ($Li_{10}SiP_2S_{12}$), and mp-696123 ($Li_{10}SnP_2S_{12}$). Structure manipulation is dealt with *pymatgen*.[53]

The DP-GEN is started with 590 structures that are generated via slightly perturbing DFT-relaxed structures. A smooth version of Deep Potential (v1.2),[31,54] which is end-to-end, i.e., capable of fitting many-component data of SSE materials with little human intervention, was used for the training step. The exploration is run on five systems step by step. Each system is composed of three or four iterations depending on its convergence. The exploration time of each system is gradually lengthened from 1000 fs to 10 000 fs. The exploration is beginning with ordered structures relaxed by DFT (i.e., structures downloaded from the Materials Project database in which the position of Ge/Si/Sn/P atoms is fixed). Then, the exploration is changed to disordered structures whose 4d sites are randomly occupied by Ge/Si/Sn/P. Exploration with the NpT ensemble

Published under license by AIP Publishing

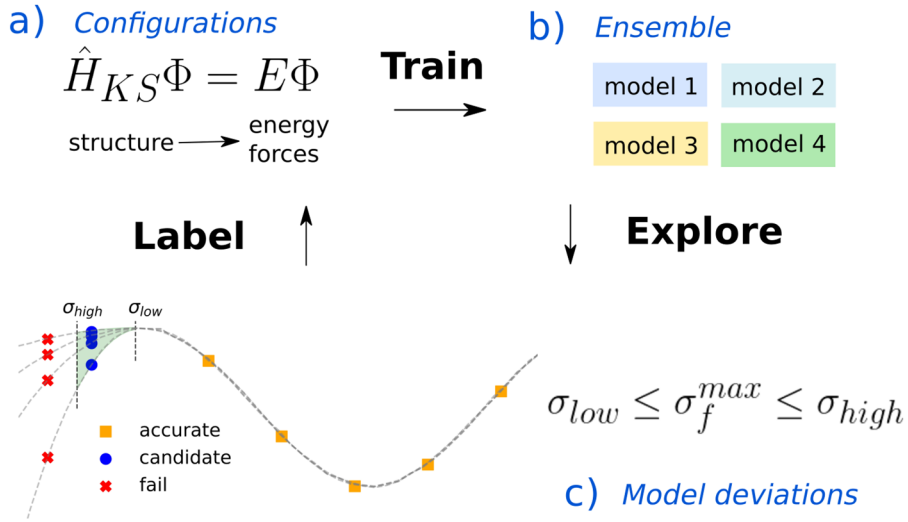

FIG. 2. Schematic illustration of the DP-GEN process. Usually, a dataset with hundreds of configurations is required to start the iteration of DP-GEN. Each DP-GEN iteration includes the three following stages: **labeling**, **training**, and **exploration**. (a) First, configurations are **labeled** by high precision single-point DFT calculations. (b) Then, an ensemble of DP models with the same architecture (i.e., number of neural network layers and nodes) but different random seeds is **trained** simultaneously using the whole dataset. (c) To **explore** larger configuration space, a few MD simulations at different thermodynamic conditions are driven by the ensemble of DP models from the previous stage. The selected candidates are labeled by DFT calculation and then added to the dataset. The exploration process is considered converged after a predetermined number of loops is reached or only a small percentage (e.g., 0.5%) of candidates are found in the last exploration iteration.

means that configurations with different lattice parameters could be automatically sampled. Finally, the exploration is performed in the systems with experimental lattice parameters. The exploration of each system is considered converged when the percentage of accurate configurations is larger than 99.5%. The detailed settings of the DP-GEN are listed in Table I. The production DP models are trained with ten times longer steps in which the number of batch and the step of learning rate decay are set to 4 000 000 and 20 000, respectively.

B. Locality test

A key assumption of most ML potentials is the *locality*. In a nutshell, ML potentials assume that properties of each atom only depend on its *local* neighboring atoms within a sphere, and the properties of the whole system could be calculated by summing up contributions from all atoms. However, this assumption may be violated in some scenarios where the long-range interactions are non-negligible. It is useful to verify the reliability of this assumption when applying DP models to SSE materials. Herein, we employed the locality test suggested by Bartók *et al.*[29] For each atom, the atom together with its neighbors within a predefined radius is fixed. Then, a random perturbation is applied over other atoms outside the sphere. The procedure is repeated several times to collect forces acting on the central atoms. The deviation of forces indicates the dependence of the atom's properties on its neighboring atoms, i.e., the locality of the system. This test is performed with different cutoff radii (5.5 Å–7.5 Å), and the procedure is run using a 2 × 2 × 2 supercell to ensure that all cells are at least twice as large as the cutoff distances.

C. DFT settings

DFT calculations were performed using the projector augmented-wave (PAW)[55,59,87] method applied in VASP 5.4.4.[56,57] The convergence test of the K-point sampling test showed that a dense reciprocal-space mesh (0.26 $Å^{-1}$) is required to ensure that forces are converged to less than 1 meV/atom. All single-point calculations were carried out with a 650 eV cutoff for plane-wave expansion, and the criterion for electronic convergence was 10^{-6} eV.

TABLE I. Exploration settings of DP-GEN iterations.

Ensemble	Iteration	Temperature (K)	Structure	Supercell
NpT	1–4	50, 100, 200, 300, 500, 700, 900, 1200	Ordered DFT-relaxed	1 × 1 × 1
NpT	5–8	300, 700, 1200	Ordered DFT-relaxed	2 × 2 × 2
NpT	9–12	50, 100, 200, 300, 500, 700, 900, 1200	Disordered DFT-relaxed	1 × 1 × 1
NpT	13–16	300, 700, 1200	Disordered DFT-relaxed	2 × 2 × 2
NVT	19–21	50, 100, 200, 300, 500, 700, 900, 1200	Ordered experiment	2 × 2 × 2

Published under license by AIP Publishing

TABLE II. Lattice parameters and unit cell volume of $Li_{10}GeP_2S_{12}$, $Li_{10}SiP_2S_{12}$, and $Li_{10}SnP_2S_{12}$ relaxed with different functional settings (PBE, LDA, PBEsol, and PBE with optB88-vdW).

Structure	Method	a (Å)	b (Å)	c (Å)	Volume (Å^3)
$Li_{10}GeP_2S_{12}$	PBE	8.591	8.879	12.977	989.1
	PBE + vdw	8.525	8.822	12.878	967.9
	LDA	8.312	8.656	12.482	897.0
	PBEsol	8.503	8.811	12.760	955.1
	SCAN	8.534	8.819	12.917	971.6
	PBE0	8.552	8.816	12.926	974.0
	Expt.[6]	8.6941	8.6941	12.5994	952.4
	Expt.[64]	8.7142	8.7142	12.6073	957.4
$Li_{10}SiP_2S_{12}$	PBE	8.774	8.774	12.599	970.0
	PBE + vdw	8.700	8.700	12.490	945.5
	LDA	8.534	8.534	12.144	884.3
	PBEsol	8.696	8.696	12.368	935.3
	SCAN	8.728	8.728	12.496	951.9
	PBE0	8.722	8.722	12.518	952.3
	Expt.[65]	8.6512	8.6512	12.5095	936.3
$Li_{10}SnP_2S_{12}$	PBE	8.835	8.835	12.882	1005.4
	PBE + vdw	8.738	8.738	12.765	974.7
	LDA	8.574	8.574	12.388	910.6
	PBEsol	8.744	8.744	12.625	965.3
	SCAN	8.774	8.774	12.759	982.3
	PBE0	8.766	8.766	12.785	982.5
	Expt.[22]	8.7057	8.7057	12.7389	965.5

To select the functional for DP models, we optimized structures with different exchange-correlation functional settings (LDA,[58] PBE,[59] PBEsol,[60] PBE with van der Waals (vdW) correction,[90] SCAN,[61] and PBE0[62,63]).

As shown in Table II, all methods except LDA overestimate the lattice volume. The lattice volumes calculated by PBEsol agree well with the experimental data. By introducing vdW correction, the results of PBE were improved. Considering the wide adoption of the PBE functional in the investigation of SSE materials[9] and the accuracy of the PBEsol functional on the prediction of lattice parameters, we trained two sets of DP models (named as DP-PBE and DP-PBEsol) to benchmark the effect of the exchange-correlation functional.

D. Molecular dynamics settings

LAMMPS[66] was employed to run all MD simulations. For each MD simulation, four DP models are used simultaneously to evaluate the model deviation (σ_f^{max}) of all snapshots in the trajectories. The tracer diffusion coefficient (D_{tr}) at each temperature is estimated by the time derivative of the mean-square displacement (MSD) of Li^+, and the block-averaged method is adopted. By default, calculations are run with experimental lattice parameters using NVT ensemble, and the time step is 2 fs. The Nose–Hoover thermostat is applied, and the relaxation time is set to 2 ps. MD simulations are run in 3D periodic cells consisting of 900 atoms ($Li_{360}Ge_{36}P_{72}S_{192}$). Detailed settings of the MD simulations are listed in Table III. As reported by the experimental work,[67] it would be reasonable to assume constant thermal expansion coefficients (3.4×10^{-5} K^{-1}) in the temperature range between 300 K and 1000 K. To the best of our knowledge, no relevant experimental data of the thermal expansion of $Li_{10}SiP_2S_{12}$ and $Li_{10}SnP_2S_{12}$ have been reported. Here, we assume that two systems have similar thermal expansion coefficients as $Li_{10}GeP_2S_{12}$. To study the finite-size effects, the unit cell of $Li_{10}GeP_2S_{12}$-type materials was scaled to various sizes ($1 \times 1 \times 1$, $2 \times 2 \times 1$, $2 \times 2 \times 2$, $3 \times 3 \times 2$, and $4 \times 4 \times 2$). To study the effect of configurational disorder, 30 cation disordered structures are generated for the MD simulations. For all MD simulations, the model deviations of snapshots are computed to ensure that energies and forces of all snapshots are reliable.

III. RESULTS AND DISCUSSION

A. Locality test

The Results of the locality test are illustrated in Fig. 3. The averaged deviations of forces are around 5 meV/Å–10 meV/Å, indicating that the assumption of the DP models is reliable for $Li_{10}GeP_2S_{12}$. The low deviations of forces acting on Li indicates the good "locality" of Li ions, and the motion of Li ions only depends on their close neighboring atoms. The relatively high deviations of Ge^{4+} and P^{5+} may due to their high charges. The long-range electrostatic forces may affect the forces on Ge and P atoms. With the increase in the cutoff radius, the local environment of an atom is better described, leading to lower deviation of forces. However, the DP models need to trade-off between accuracy and computational cost. In the $Li_{10}GeP_2S_{12}$-type materials, we found that 6 Å would be sufficiently accurate to describe the diffusion process, which is adopted in this work as follows. Thus, it would be useful to incorporate a long-range effect in the machine learning potentials to improve the description of the interatomic interaction. In conclusion, the locality test shows that

TABLE III. MD settings for the investigation of different factors, i.e., the density functional, simulation time and cell size, thermal expansion, and configurational disorder, are listed. N_{atom} means the number of atoms in the systems.

Factor	Time (ns)	N_{atom}	Temperature (K)
Density functional	1	900	400, 500, 666, 800, 1000
Simulation time and cell size	10	50, 200, 400, 900, 1600	300, 400, 500, 600
Thermal expansion	1	900	500, 666, 800, 1000
Configurational disorder	1	900	300, 400, 500, 666

Published under license by AIP Publishing

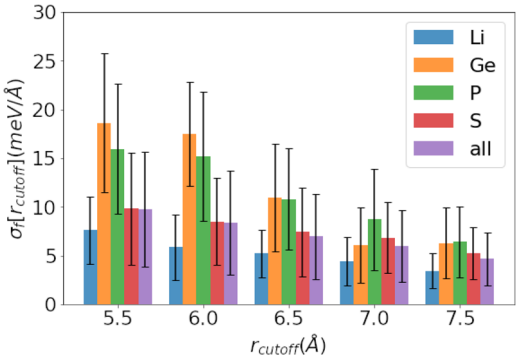

FIG. 3. The locality test of $Li_{10}GeP_2S_{12}$. The averaged force deviation (σ_f) of each element, calculated with different cutoff radii, is displayed. The error bars correspond to the standard deviation of the force data.

the end-to-end deep potential models would be accurate enough to investigate the diffusion of Li in $Li_{10}GeP_2S_{12}$-type materials.

B. DP-GEN iteration

To better illustrate the DP-GEN procedure, it is worth taking a thorough look at the exploration results of each iteration. Here, we study $Li_{10}GeP_2S_{12}$ in depth as a benchmark due to its importance and extensive previous work.

Figure 4 shows the distribution of σ_f^{max} at different temperatures in the first four iterations. And Table IV displays the percentage of the accurate, candidate, and failed groups of configurations in each iteration. In the first iteration, it is not surprising that the trajectories given by the preliminary models include lots of unreasonable configurations and high-temperature simulations blow up very quickly. A large fraction of the snapshots sampled in this iteration have a σ_f^{max} larger than 0.4 eV/Å [Fig. 4(a)]. A large portion of the candidates with σ_f^{max} fallen in the selection range and selected for labeling are from low-temperature simulations. This situation is drastically improved after just adding 300 labeled configurations to the training dataset. In the second iteration, most low-temperature snapshots are labeled as "accurate" and the majority of newly selected snapshots come from higher-temperature simulations. Going from the second iteration to the third and the fourth, although the time duration of the simulation is extended (i.e., 1000 fs, 5000 fs, and 10 000 fs, respectively), most snapshots have their σ_f^{max} value at a satisfactory level, demonstrating a quick convergence of the DP-GEN process. After four iterations, the models have converged in the original cell (50 atoms), i.e., the percentage of candidates being ~1%.

The fifth to eighth iterations are performed with 2 × 2 × 2 supercells (200 atoms) with the percentage of candidates gradually decreasing to 0.6%. Then, the exploration moves to disorder structures from the ninth to the sixteenth iterations. Due to the similarity of the structures, only a small percentage of new configurations are labeled as "candidate" in these iterations. In the last three

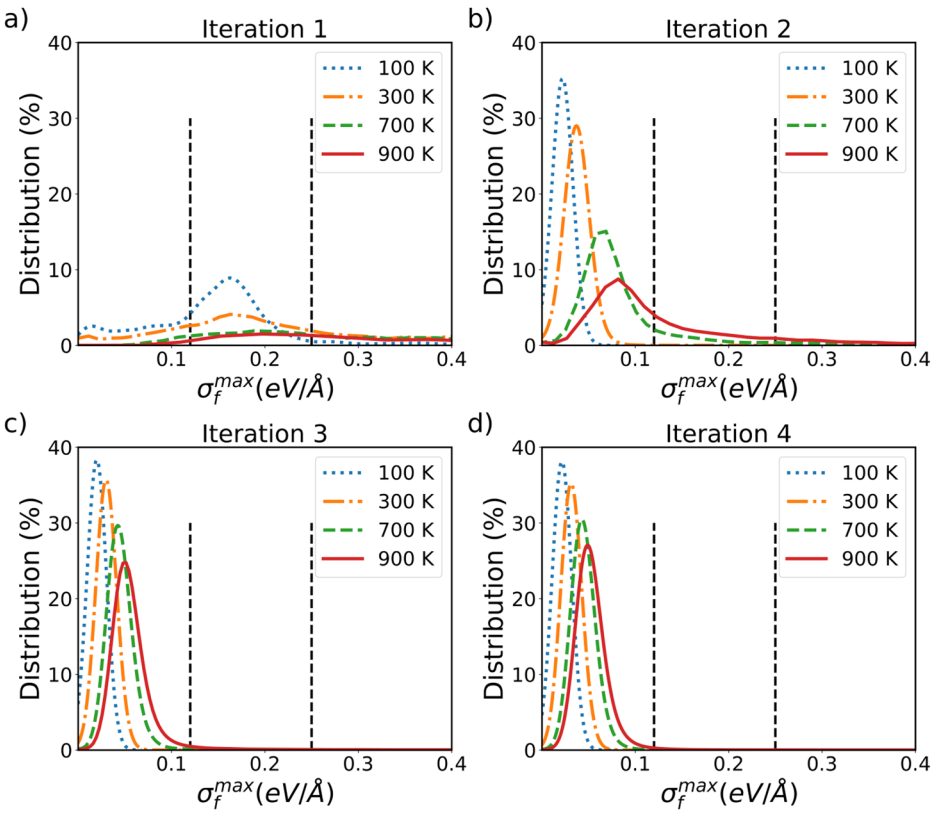

FIG. 4. For $Li_{10}GeP_2S_{12}$, distribution of maximum deviation of force (σ_f^{max}) from iteration 1–4. Distribution of deviation values at four temperatures is plotted, and the two vertical lines (dashed) correspond to the lower and upper bound of the selection criteria (0.12 eV/Å and 0.25 eV/Å).

Published under license by AIP Publishing

TABLE IV. Percentage of accurate, candidate, and failed configurations in each iteration. Data are labeled with the PBE functional.

Type	1	2	3	4	5	6	7	8	9	10	11	12	13	14	15	16	17	18	19
Candidate	36.57	7.15	1.40	0.78	6.11	7.95	2.63	3.76	0.23	0.13	0.15	0.03	0.67	0.83	1.10	1.28	4.47	0.71	0.95
Accurate	16.14	81.57	95.95	98.74	92.62	91.41	97.08	96.10	99.75	99.86	99.84	99.96	99.31	99.07	98.85	98.69	95.46	99.19	99.03
Failed	47.28	11.26	2.64	0.47	1.26	0.63	0.27	0.12	0.00	0.00	0.00	0.00	0.01	0.08	0.03	0.02	0.08	0.11	0.02

iterations, the exploration is run with NVT using the experimental lattice parameters, the same setting we use in the calculation of diffusion coefficients. Still, a few candidates arise in these iterations, yet the DP models converge within three iterations. Similar trends are found in $Li_{10}SiP_2S_{12}$ and $Li_{10}SnP_2S_{12}$ systems.

Finally, around 4000 configurations in total are collected via DP-GEN automatically to train the DP models. The protocol could be further improved, e.g., by merging the exploration process of ordered and disordered structures or training the universal DP models for the "Li-SiGeSn-PS" system.

C. Accuracy and speed test of DP models

To ensure how much the DP models could speed up the simulation without losing the DFT-level accuracy, the accuracy and speed test are performed on the whole DFT dataset. As shown in Table V, the root-mean-square errors (RMSEs) of energies per atom and forces are around 2 meV/atom and 80 meV/Å for two sets of models using PBE and PBEsol functionals, and they have similar accuracy. The diagnostic plots between DFT and DP models are shown in Fig. 5. The low standard deviations of the four models suggest that all potentials share similar accuracy, and the DP-GEN scheme gives consistent errors for three different systems.

The speed test is run on one NVIDIA V100 GPU, and the results are reported in Fig. 6. It only takes around 4 h to simulate 900-atom systems for 1 ns, and the computational cost of DP scales nearly linearly with the system size. The high accuracy and extraordinary speed make deep potential a powerful tool for large-scale atomic simulation.

D. Simulation protocol for diffusion coefficients

1. Effect of finite-size and simulation time

Previous studies[23] based on AIMD have suggested that a 200 ps MD simulation would be sufficient to ensure the convergence of diffusivity at high temperatures (>600 K), and this is confirmed in Fig. 7(a). Diffusion coefficients above the level of 10^{-10} m^2/s (400 K and 500 K) reach very small variances and converge within 1 ns. Since the diffusivity decreases exponentially with temperature, the statistics of diffusion processes at room temperature require longer time to converge. At 300 K, extending the simulation to 10 ns ensures convergence of all diffusivity data with an uncertainty of 10^{-12} m^2/s. Thus, the time scale of 10 ns is required for the simulation of room temperature diffusion processes.

The system-size dependence of the diffusion coefficient and viscosity from MD simulations with periodic boundary conditions is a classic topic and has been extensively discussed by, e.g., Yeh and Hummer.[68] Following the test of simulation time, analysis of the size effect is performed with 10 ns trajectories. Here, as shown in Fig. 7(b), a 2 × 2 × 1 supercell size (200 atoms), which was used in most previous AIMD simulations of SSE materials,[11,13] overestimates diffusion coefficients by 10–100 times. The diffusion coefficients start to converge when systems are enlarged to 2 × 2 × 2 supercells (400 atoms). However, this system still significantly overestimates diffusion coefficients at 300 K. By expanding the system to 900 atoms and 1600 atoms, we notice that the difference of diffusion coefficients between them is around 3×10^{-12} m^2/s. Taking into account the results of the convergence test and speed test, we will run simulations with 900-atom systems for 1 ns for high temperatures (>400 K), and the simulation is lengthened to 10 ns when studying the diffusion process at room temperature. This setting may still slightly overestimate the diffusion coefficient at 300 K, but it should give the correct magnitude of diffusion coefficients.

TABLE V. Root-mean square errors of the energies per atom (meV/atom) and forces (meV/Å) of the DP-PBE and DP-PBEsol on the whole dataset generated from the DP-GEN scheme. The standard deviations are evaluated using an ensemble of four models.

Model	RMSEs	$Li_{10}GeP_2S_{12}$	$Li_{10}SiP_2S_{12}$	$Li_{10}SnP_2S_{12}$
DP-PBE	E	1.65 ± 0.03	1.82 ± 0.01	2.53 ± 0.02
	f	82.4 ± 0.91	82.7 ± 0.19	92.5 ± 0.39
DP-PBEsol	E	1.33 ± 0.06	1.33 ± 0.01	1.27 ± 0.01
	f	79.6 ± 1.57	77.7 ± 0.39	77.9 ± 0.29

2. Effect of density functional on diffusion coefficient

The quality of the interatomic potential depends on the DFT data. To the best of our knowledge, though it is suggested that the interatomic potentials labeled by different functionals may give different diffusion coefficients,[38] there has not been any relevant benchmark report. The diffusion coefficients calculated by DP-PBE and DP-PBEsol models are displayed in Fig. 8. Simulated with the experimental lattice parameters, both sets of DP models give similar diffusion coefficients. The consistency of the diffusion coefficients implies that though different methods give different lattice parameters (the lattice parameters computed by PBE are 3% larger than that computed by PBEsol), they do not significantly affect the calculated diffusion coefficients.

3. Effect of thermal expansion

The lattice parameter is known to significantly affect the diffusion process.[9,69,70] Ong *et al.*[9] reported the effect of expansion or contraction of the lattice on calculated diffusion coefficients at the same temperature. The thermal expansion is relatively small at low temperatures (less than 1%); thus, we only evaluate the effect at the

Published under license by AIP Publishing

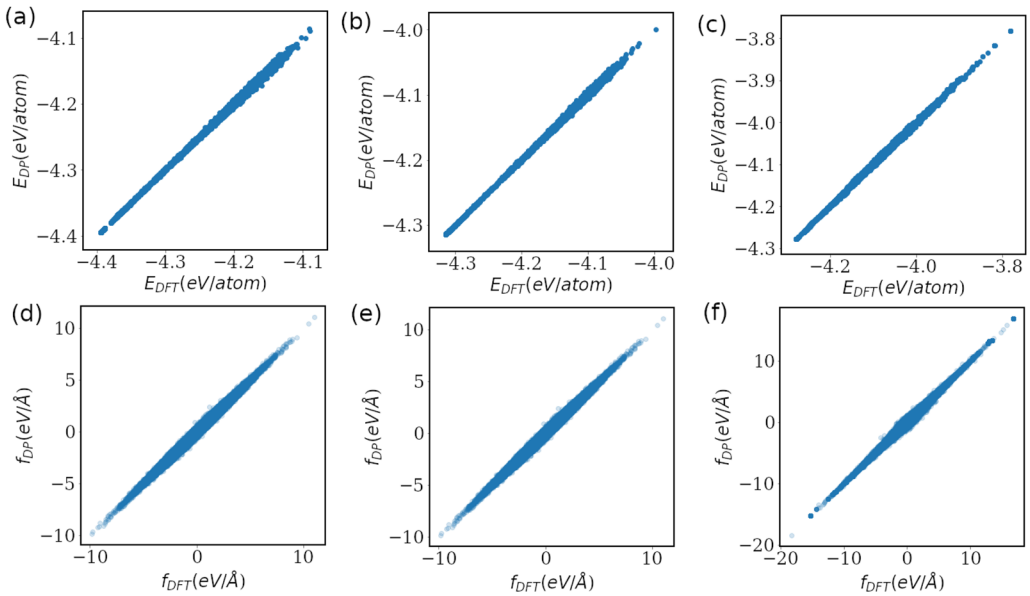

FIG. 5. Comparison of the energies and forces computed by DP models and DFT of the three systems $Li_{10}SiP_2S_{12}$ [(a) and (d)], $Li_{10}GeP_2S_{12}$ [(b) and (e)], and $Li_{10}SnP_2S_{12}$ [(c) and (f)], respectively.

high temperature regime (>700 K). It is shown in Fig. 9 that at high temperatures, the thermal expansion already leads to noticeable differences in the computed diffusion coefficients. Thus, the effect of thermal expansion should be considered at the whole temperature range.

To set up an automatic workflow, it is worth exploring whether DP models could predict the thermal expansion coefficients. To obtain the lattice parameters at different temperatures, we equilibrated the simulation cell with the N*p*T ensemble for 1 ns at different temperatures and averaged all configurations of trajectories to calculate the lattice parameters. The $Li_{10}GeP_2S_{12}$-type materials belong to the tetragonal crystal lattice of which the lattice parameter *a* is equivalent to lattice parameter *b*, and thus, the thermal expansions of lattice parameters a and c are presented in Fig. 10. Weber *et al.*[67] found that lattice parameters *a* and *c* exhibit linear thermal expansion below 700 K and show slightly anisotropic expansion at higher temperature. Here, we focus on the linear expansion region that is of practical interest. The thermal expansion coefficient (α^L_{300K}) calculated by DP-PBE and DP-PBEsol are both 3.2×10^{-5} K^{-1}, consistent with the value 3.5×10^{-5} K^{-1} from the experiment.[67] Thus, we conclude that the N*p*T simulations could be adopted in the protocol to estimate thermal expansion coefficients of SSE materials for the accurate simulation of diffusion processes.

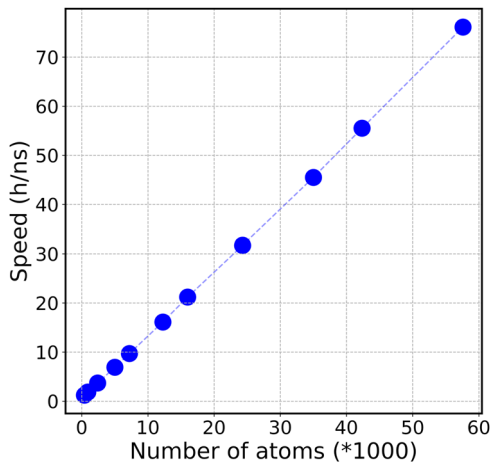

FIG. 6. Speed test of DP models on a NVIDIA V100 GPU. The system ($Li_{10}GeP_2S_{12}$) is scaled to different sizes to test the required simulation time.

4. Effect of configurational disorder

It has been suggested that the disordered arrangement in SSE materials may improve diffusion coefficients.[45–48] However, an atomic insight based on sufficient MD simulations is still lacking. To sample cation disordered configurations, a large simulation system is required, which is beyond the ability of AIMD. By including the disordered configurations in DP-GEN iterations, our DP models are able to accurately simulate disordered configurations. In this test, 30 disordered configurations with 900 atoms ($Li_{360}M_{36}P_{72}S_{432}$, M = Si, Ge, Sn) are randomly generated to compute diffusion coefficients.

In Fig. 11, we plot diffusion coefficients calculated with cation site disordered structures. At low temperatures, the disorder of cations (Ge^{4+} and P^{5+}) increases the diffusion coefficients by 2–4 times. The diffusion process of Li in the $Li_{10}GeP_2S_{12}$-type materials could be described as the jumping events of Li between several connected sites, each with a unique local environment. A simplified model to explain the effect of disorder is that the disordered arrangement "flatten" the potential energy surface between these sites,[46] i.e., decrease the possible maximum energy barriers. Due to the speed-up

Published under license by AIP Publishing

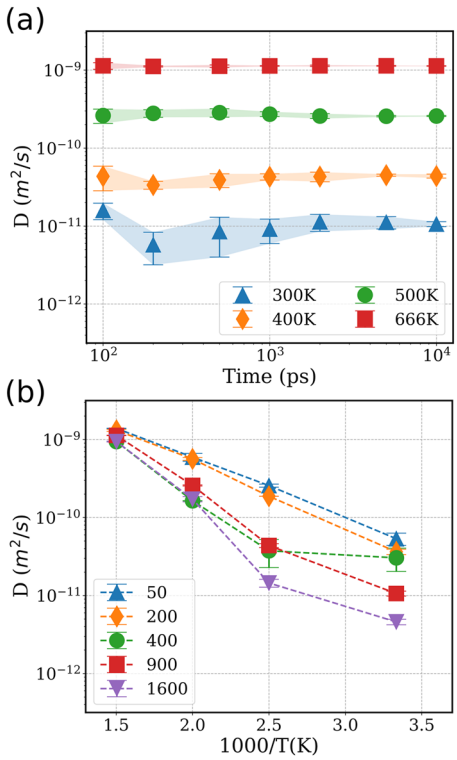

FIG. 7. The convergence test of diffusion coefficients for $Li_{10}SiP_2S_{12}$. Data are computed with different (a) simulation time lengths (100 ps, 200 ps, 500 ps, 1 ns, 2 ns, 5 ns, and 10 ns) and (b) system sizes (50, 200, 400, 900, and 1600 atoms).

of the rate-determining step, the jumping process is enhanced, leading to the improvement of diffusion coefficients. The effect is not very significant at high temperatures because the benefit is relatively small in the systems with high diffusion coefficients.

Surprisingly, $Li_{10}GeP_2S_{12}$ and $Li_{10}SiP_2S_{12}$ benefit from the disorder while configurational disorder decreases diffusion coefficients of $Li_{10}SnP_2S_{12}$. These data may explain the fact that though $Li_{10}SnP_2S_{12}$ has the largest volume among the three materials, the

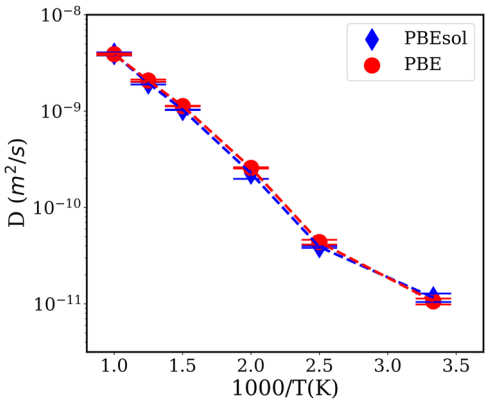

FIG. 8. Diffusion coefficients of $Li_{10}SiP_2S_{12}$ simulated with DP-PBE and DP-PBEsol.

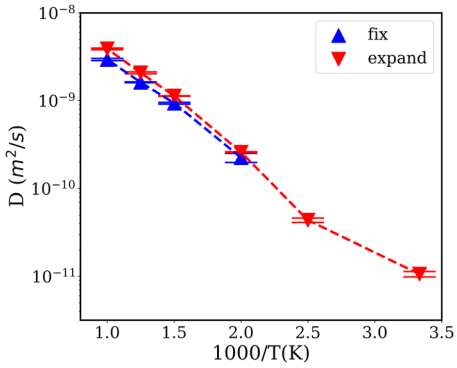

FIG. 9. Diffusion coefficients of $Li_{10}SiP_2S_{12}$; the "fix" and "expand" data correspond to simulations at different temperatures with fixed lattice parameters and lattice parameters assuming linear thermal expansion, respectively.

configurational disorder of this material decreases its diffusion coefficients.

Besides, it is interesting that diffusion coefficients of the disordered systems seem to follow the Arrhenius relationship at low temperatures, while the ordered systems do not. According to the classification of the three kinds of diffusion behaviors mentioned in Fig. 1, one possible reason is that the ordered structures may undergo phase transition when they are cooled down. Another possible reason is that the diffusion mechanism may change, e.g., the diffusion path across the *ab* plane is shut.

To investigate the difference between ordered and disordered structures, we analyze the radial distribution functions (RDF) of the three systems and the results are plotted in Fig. 12. For all three systems, configurational disorder does not change the RDF of Li–Li and Li–S, while it slightly changes the RDF of Li–P (M = Si/Ge). Interestingly, the RDF of Li-M (M = Si/Ge/Sn) of $Li_{10}SnP_2S_{12}$ significantly changed due to the disorder compared to $Li_{10}SiP_2S_{12}$ and $Li_{10}GeP_2S_{12}$. The rearrangement of Sn and P sites may change the local environment of Li sites in $Li_{10}SnP_2S_{12}$, leading to significant

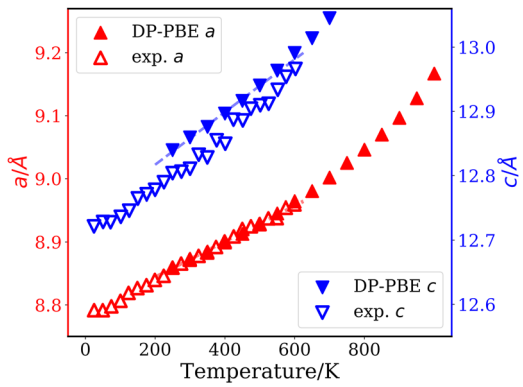

FIG. 10. Thermal expansion of $Li_{10}GeP_2S_{12}$. The lattice parameters *a* and *c* are shown. The experimental data are extracted from the study of Weber *et al.*[67] The lattice parameters at different temperatures are estimated by the DP-PBE models. The dashed lines are the fitting range of thermal expansion coefficients.

Published under license by AIP Publishing

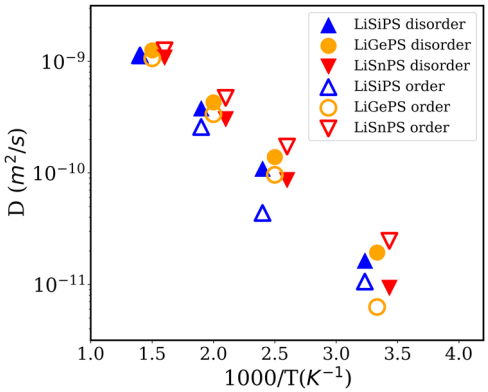

FIG. 11. Diffusion coefficients of $Li_{10}GeP_2S_{12}$, $Li_{10}SiP_2S_{12}$, and $Li_{10}SnP_2S_{12}$ averaged from cation site ordered/disordered configurations. Note that the set of temperatures studied are the same for the three materials and the data of $Li_{10}SiP_2S_{12}$ and $Li_{10}SnP_2S_{12}$ are slightly shifted to left and right for better visualization, respectively.

energy differences among Li sites and thus, the suppression of diffusion processes. We also notice that for both ordered and disordered systems, the RDF of Li–P and Li–Ge in $Li_{10}GeP_{12}S_{12}$ are quite similar, indicating that the Li sites may have smaller energy differences than the other two systems, which is beneficial to the diffusion process. The physics of $Li_{10}SnP_2S_{12}$ and the possible different transition behaviors between ordered and disordered structures require future analysis of the diffusion process, including the statistics of jumping events between local environments.

E. Comparison to experiment

Based on the above investigation, we concluded that the effect of thermal expansion and configurational disorder shall be considered to obtain accurate simulation results. Our results, data of previous AIMD simulations and experiments, are plotted in Fig. 13 The computed diffusion coefficients of the three systems ($Li_{10}SiP_2S_{12}$, $Li_{10}GeP_2S_{12}$, and $Li_{10}SnP_2S_{12}$) are $16 \pm 2 \times 10^{-12}$ m^2/s, $19 \pm 2 \times 10^{-12}$ m^2/s, and $9 \pm 2 \times 10^{-12}$ m^2/s. In addition, the experimental data[17] are $5.8 \pm 2 \times 10^{-12}$ m^2/s, $4.1 \pm 2 \times 10^{-12}$ m^2/s, and $3.1 \pm 2 \times 10^{-12}$ m^2/s, respectively. The DP models overestimate the diffusion coefficients at room temperature for around 5×10^{-12} m^2/s–15×10^{-12} m^2/s.

The difference between experiments and simulation data computed by DP models may be due to the following reasons: First, according to the *interlaboratory reproducibility* study by Zeier and the co-workers,[71] the experimental reported ionic conductivities have a uncertainty up to 4.5 mS/cm [corresponding to an

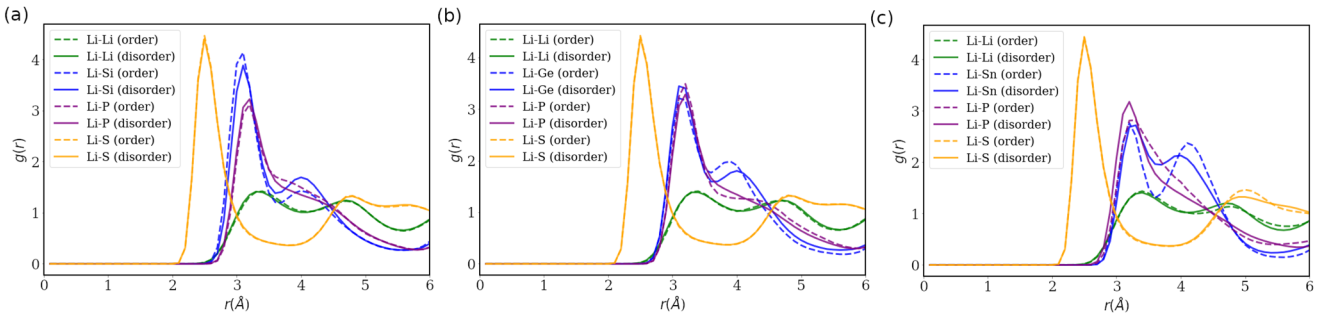

FIG. 12. Radial distribution functions (RDF) of Li and other ions in $Li_{10}SiP_2S_{12}$ (a), $Li_{10}GeP_2S_{12}$ (b), and $Li_{10}SnP_2S_{12}$ (c). RDF data of ordered and disordered configurations are averaged from five trajectories. The dashed and solid lines correspond to ordered and disordered structures, respectively.

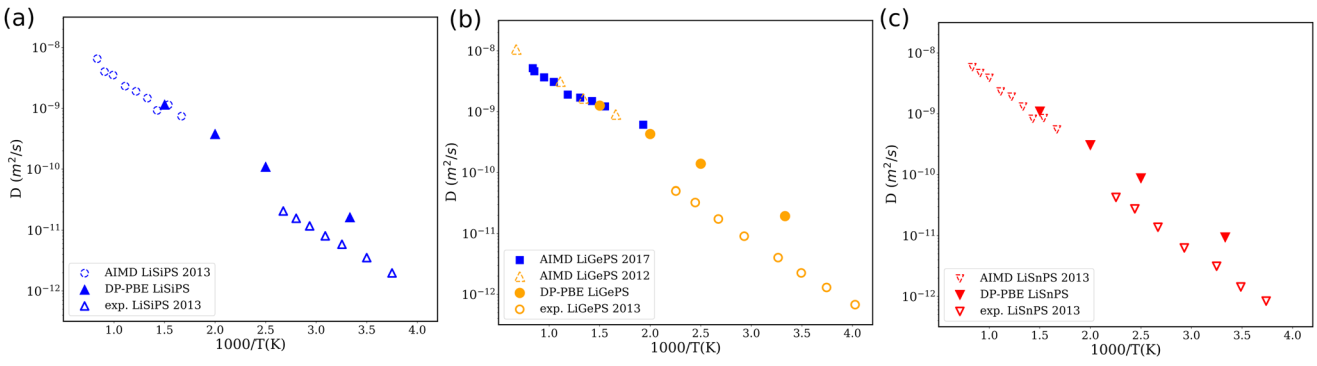

FIG. 13. Diffusion coefficients of the $Li_{10}SiP_2S_{12}$ (a), $Li_{10}GeP_2S_{12}$ (b), and $Li_{10}SnP_2S_{12}$ (c) obtained from our DP-PBE models, previous AIMD simulations,[11,16] and experimental solid-state NMR results.[17]

Published under license by AIP Publishing

uncertainty of 1×10^{-12} m^2/s–5×10^{-12} m^2/s for $Li_{10}GeP_2S_{12}$-type materials)], which is similar to the overestimation given by the DP models. The uncertainty of the experimental measurement may be due to the synthesize settings and the impurity of materials,[22,65] which usually decrease the diffusion coefficients. Second, as shown by the test of the finite-size effect, we would expect a slight overestimation of our diffusion coefficients that are sampled by 900-atom systems. Third, the models trained in this work could still be improved in several aspects, e.g., by including the long-range interactions and trading off between accuracy and computational cost. Despite these, our DP models presented in this work achieve state-of-the-art performance on the simulation of the diffusion processes of $Li_{10}GeP_2S_{12}$-type materials.

IV. CONCLUSION

In this work, we present a systematic benchmark study for the generation, validation, and application of DP-GEN for $Li_{10}GeP_2S_{12}$-type materials. We provide an efficient automated protocol to generate DP models, and the key properties (accuracy, locality, thermal expansion, and the diffusion coefficient) of the DP models are examined. With the DP models, we establish a reliable protocol to compute the diffusion coefficients in a wide temperature range (300 K–1000 K). The results show that current protocols based on AIMD simulation significantly overestimate diffusion coefficients due to the finite-size effect and the ignorance of configurational disorder. Although our computed diffusion coefficients still slightly overestimate the diffusion coefficients, the errors are within experimental uncertainty. The protocol should be sufficiently accurate to be applied to run simulations to understand the diffusion mechanisms of SSE materials. With the verified protocols, we notice that the effect of configurational disorder may depend on the materials, i.e., $Li_{10}SnP_2S_{12}$ shows a different behavior from $Li_{10}GeP_2S_{12}$ and $Li_{10}SiP_2S_{12}$. The data generated in this work could be a starting point for research of doping and replacement of $Li_{10}GeP_2S_{12}$-type materials in the future.[72,76–80]

ACKNOWLEDGMENTS

J.H. and J.C. acknowledge the National Natural Science Foundation of China (Grants Nos. 21861132015, 21991150, 21991151, 91745103, and 22021001) for funding support. J.H. and J.Z. were supported by the National Key Research and Development Program of China (Grant No. 2017YFB0102000). L.Z. and W.E were supported, in part, by a gift from iFlytek to Princeton University (ONR Grant No. N00014-13-1-0338) and the Center Chemistry in Solution and at Interfaces (CSI) funded by the DOE Award No. DE-SC0019394. H.W. was supported by the National Science Foundation of China (Grant No. 11871110), the National Key Research and Development Program of China (Grant Nos. 2016YFB0201200 and 2016YFB0201203), and Beijing Academy of Artificial Intelligence (BAAI).

DATA AVAILABILITY

All DP models and the labeled DFT data could be downloaded from http://dplibrary.deepmd.net/.

REFERENCES

[1] J. B. Goodenough and K.-S. Park, "The Li-ion rechargeable battery: A perspective," J. Am. Chem. Soc. **135**, 1167–1176 (2013).
[2] J.-M. Tarascon and M. Armand, "Issues and challenges facing rechargeable lithium batteries," in *Materials for Sustainable Energy: A Collection of Peer-Reviewed Research and Review Articles from Nature Publishing Group* (World Scientific, 2011), pp. 171–179.
[3] S. Chu and A. Majumdar, "Opportunities and challenges for a sustainable energy future," Nature **488**, 294 (2012).
[4] Y.-S. Hu, "Batteries: Getting solid," Nat. Energy **1**, 16042 (2016).
[5] Z. Zhang, Y. Shao, B. Lotsch, Y.-S. Hu, H. Li, J. Janek, L. F. Nazar, C.-W. Nan, J. Maier, M. Armand *et al.*, "New horizons for inorganic solid state ion conductors," Energy Environ. Sci. **11**, 1945–1976 (2018).
[6] N. Kamaya, K. Homma, Y. Yamakawa, M. Hirayama, R. Kanno, M. Yonemura, T. Kamiyama, Y. Kato, S. Hama, K. Kawamoto *et al.*, "A lithium superionic conductor," Nat. Mater. **10**, 682 (2011).
[7] R. Murugan, V. Thangadurai, and W. Weppner, "Fast lithium ion conduction in garnet-type $Li_7La_3Zr_2O_{12}$," Angew. Chem., Int. Ed. **46**, 7778–7781 (2007).
[8] Y. Seino, T. Ota, K. Takada, A. Hayashi, and M. Tatsumisago, "A sulphide lithium super ion conductor is superior to liquid ion conductors for use in rechargeable batteries," Energy Environ. Sci. **7**, 627–631 (2014).
[9] S. P. Ong, Y. Mo, W. D. Richards, L. Miara, H. S. Lee, and G. Ceder, "Phase stability, electrochemical stability and ionic conductivity of the $Li_{10\pm1}MP_2X_{12}$ (M = Ge, Si, Sn, Al or P, and X = O, S or Se) family of superionic conductors," Energy Environ. Sci. **6**, 148–156 (2013).
[10] G. Ceder, S. P. Ong, and Y. Wang, "Predictive modeling and design rules for solid electrolytes," MRS Bull. **43**, 746–751 (2018).
[11] Y. Mo, S. P. Ong, and G. Ceder, "First principles study of the $Li_{10}GeP_2S_{12}$ lithium super ionic conductor material," Chem. Mater. **24**, 15–17 (2012).
[12] R. Car and M. Parrinello, "Unified approach for molecular dynamics and density-functional theory," Phys. Rev. Lett. **55**, 2471 (1985).
[13] X. He, Y. Zhu, and Y. Mo, "Origin of fast ion diffusion in super-ionic conductors," Nat. Commun. **8**, 15893 (2017).
[14] A. M. Nolan, Y. Zhu, X. He, Q. Bai, and Y. Mo, "Computation-accelerated design of materials and interfaces for all-solid-state lithium-ion batteries," Joule **2**, 2016 (2018).
[15] A. Van der Ven and G. Ceder, "Lithium diffusion in layered Li_xCoO_2," Electrochem. Solid-State Lett. **3**, 301–304 (2000).
[16] A. Marcolongo and N. Marzari, "Ionic correlations and failure of Nernst-Einstein relation in solid-state electrolytes," Phys. Rev. Mater. **1**, 025402 (2017).
[17] A. Kuhn, J. Köhler, and B. V. Lotsch, "Single-crystal X-ray structure analysis of the superionic conductor $Li_{10}GeP_2S_{12}$," Phys. Chem. Chem. Phys. **15**, 11620 (2013).
[18] J. B. Boyce and B. A. Huberman, "Superionic conductors: Transitions, structures, dynamics," Phys. Rep. **51**, 189–265 (1979).
[19] M. Tachez, J.-P. Malugani, R. Mercier, and G. Robert, "Ionic conductivity of and phase transition in lithium thiophosphate Li_3PS_4," Solid State Ionics **14**, 181–185 (1984).
[20] O. Kwon, M. Hirayama, K. Suzuki, Y. Kato, T. Saito, M. Yonemura, T. Kamiyama, and R. Kanno, "Synthesis, structure, and conduction mechanism of the lithium superionic conductor $Li_{10+\delta}Ge_{1+\delta}P_{2-\delta}S_{12}$," J. Mater. Chem. A **3**, 438–446 (2015).
[21] R. Kanno and M. Murayama, "Lithium ionic conductor thio-LISICON: The Li_2S-GeS_2-P_2S_5 system," J. Electrochem. Soc. **148**, A742–A746 (2001).
[22] P. Bron, S. Johansson, K. Zick, J. Schmedt auf der Günne, S. Dehnen, and B. Roling, "$Li_{10}SnP_2S_{12}$: An affordable lithium superionic conductor," J. Am. Chem. Soc. **135**, 15694–15697 (2013).
[23] X. He, Y. Zhu, A. Epstein, and Y. Mo, "Statistical variances of diffusional properties from *ab initio* molecular dynamics simulations," npj Comput. Mater. **4**, 18 (2018).
[24] R. Xiao, H. Li, and L. Chen, "Candidate structures for inorganic lithium solid-state electrolytes identified by high-throughput bond-valence calculations," J. Materiomics **1**, 325–332 (2015).

Published under license by AIP Publishing

[25]L. Kahle, A. Marcolongo, and N. Marzari, "Modeling lithium-ion solid-state electrolytes with a pinball model," Phys. Rev. Mater. **2**, 065405 (2018).
[26]R. Kobayashi, Y. Miyaji, K. Nakano, and M. Nakayama, "High-throughput production of force-fields for solid-state electrolyte materials," APL Mater. **8**, 081111 (2020).
[27]H.-X. Li, X.-Y. Zhou, Y.-C. Wang, and H. Jiang, "Theoretical study of Na^+ transport in the solid-state electrolyte Na_3OBr based on deep potential molecular dynamics," Inorg. Chem. Front. **8**, 425 (2020).
[28]J. Behler and M. Parrinello, "Generalized neural-network representation of high-dimensional potential-energy surfaces," Phys. Rev. Lett. **98**, 146401 (2007).
[29]A. P. Bartók, M. C. Payne, R. Kondor, and G. Csányi, "Gaussian approximation potentials: The accuracy of quantum mechanics, without the electrons," Phys. Rev. Lett. **104**, 136403 (2010).
[30]N. Artrith, A. Urban, and G. Ceder, "Efficient and accurate machine-learning interpolation of atomic energies in compositions with many species," Phys. Rev. B **96**, 014112 (2017).
[31]L. Zhang, J. Han, H. Wang, W. Saidi, R. Car, and W. E, "End-to-end symmetry preserving inter-atomic potential energy model for finite and extended systems," in *Advances in Neural Information Processing Systems* (Curran Associates, Inc., 2018), Vol. 31, pp. 4436–4446.
[32]N. Artrith, A. Urban, and G. Ceder, "Constructing first-principles phase diagrams of amorphous Li_xSi using machine-learning-assisted sampling with an evolutionary algorithm," J. Chem. Phys. **148**, 241711 (2018).
[33]V. L. Deringer, C. Merlet, Y. Hu, T. H. Lee, J. A. Kattirtzi, O. Pecher, G. Csányi, S. R. Elliott, and C. P. Grey, "Towards an atomistic understanding of disordered carbon electrode materials," Chem. Commun. **54**, 5988–5991 (2018).
[34]S. Fujikake, V. L. Deringer, T. H. Lee, M. Krynski, S. R. Elliott, and G. Csányi, "Gaussian approximation potential modeling of lithium intercalation in carbon nanostructures," J. Chem. Phys. **148**, 241714 (2018).
[35]V. Lacivita, N. Artrith, and G. Ceder, "Structural and compositional factors that control the Li-ion conductivity in LiPON electrolytes," Chem. Mater. **30**, 7077–7090 (2018).
[36]W. Li, Y. Ando, E. Minamitani, and S. Watanabe, "Study of Li atom diffusion in amorphous Li_3PO_4 with neural network potential," J. Chem. Phys. **147**, 214106 (2017).
[37]Z. Deng, C. Chen, X.-G. Li, and S. P. Ong, "An electrostatic spectral neighbor analysis potential for lithium nitride," npj Comput. Mater. **5**, 75 (2019).
[38]A. Marcolongo, T. Binninger, F. Zipoli, and T. Laino, "Simulating diffusion properties of solid-state electrolytes via a neural network potential: Performance and training scheme," ChemSystemsChem **2**, e1900031 (2019).
[39]N. Bernstein, G. Csányi, and V. L. Deringer, "De novo exploration and self-guided learning of potential-energy surfaces," npj Comput Mater **5**, 99 (2019).
[40]C. Nyshadham, M. Rupp, B. Bekker, A. V. Shapeev, T. Mueller, C. W. Rosenbrock, G. Csányi, D. W. Wingate, and G. L. Hart, "Machine-learned multi-system surrogate models for materials prediction," npj Comput. Mater. **5**, 51 (2019).
[41]V. L. Deringer, D. M. Proserpio, G. Csányi, and C. J. Pickard, "Data-driven learning and prediction of inorganic crystal structures," Faraday Discuss. **211**, 45–59 (2018).
[42]B. Mortazavi, E. V. Podryabinkin, I. S. Novikov, S. Roche, T. Rabczuk, X. Zhuang, and A. V. Shapeev, "Efficient machine-learning based interatomic potentials for exploring thermal conductivity in two-dimensional materials," J. Phys.: Mater. **3**, 02LT02 (2020).
[43]E. V. Podryabinkin, E. V. Tikhonov, A. V. Shapeev, and A. R. Oganov, "Accelerating crystal structure prediction by machine-learning interatomic potentials with active learning," Phys. Rev. B **99**, 064114 (2019).
[44]K. Gubaev, E. V. Podryabinkin, and A. V. Shapeev, "Machine learning of molecular properties: Locality and active learning," J. Chem. Phys. **148**, 241727 (2018).
[45]A. R. Stamminger, B. Ziebarth, M. Mrovec, T. Hammerschmidt, and R. Drautz, "Ionic conductivity and its dependence on structural disorder in halogenated argyrodites Li_6PS_5X (X = Br, Cl, I)," Chem. Mater. **31**, 8673–8678 (2019).
[46]S. Ohno, B. Helm, T. Fuchs, G. Dewald, M. A. Kraft, S. P. Culver, A. Senyshyn, and W. G. Zeier, "Further evidence for energy landscape flattening in the superionic argyrodites $Li_{6+x}P_{1-x}M_xS_5I$ (M = Si, Ge, Sn)," Chem. Mater. **31**, 4936–4944 (2019).
[47]L. Zhou, A. Assoud, A. Shyamsunder, A. Huq, Q. Zhang, P. Hartmann, J. Kulisch, and L. F. Nazar, "An entropically stabilized fast-ion conductor: $Li_{3.25}[Si_{0.25}P_{0.75}]S_4$," Chem. Mater. **31**, 7801–7811 (2019).
[48]I. Hanghofer, M. Brinek, S. L. Eisbacher, B. Bitschnau, M. Volck, V. Hennige, I. Hanzu, D. Rettenwander, and H. M. R. Wilkening, "Substitutional disorder: Structure and ion dynamics of the argyrodites Li_6PS_5Cl, Li_6PS_5Br and Li_6PS_5I," Phys. Chem. Chem. Phys. **21**, 8489–8507 (2019).
[49]L. Zhang, D.-Y. Lin, H. Wang, R. Car, and W. E, "Active learning of uniformly accurate interatomic potentials for materials simulation," Phys. Rev. Mater. **3**, 023804 (2019).
[50]Y. Zhang, H. Wang, W. Chen, J. Zeng, L. Zhang, H. Wang, and W. E, "DP-GEN: A concurrent learning platform for the generation of reliable deep learning based potential energy models," Comput. Phys. Commun. **253**, 107206 (2020).
[51]A. Jain, S. P. Ong, G. Hautier, W. Chen, W. D. Richards, S. Dacek, S. Cholia, D. Gunter, D. Skinner, G. Ceder *et al.*, "Commentary: The materials project: A materials genome approach to accelerating materials innovation," APL Mater. **1**, 011002 (2013).
[52]S. P. Ong, S. Cholia, A. Jain, M. Brafman, D. Gunter, G. Ceder, and K. A. Persson, "The materials application programming interface (API): A simple, flexible and efficient api for materials data based on representational state transfer (REST) principles," Comput. Mater. Sci. **97**, 209–215 (2015).
[53]S. P. Ong, W. D. Richards, A. Jain, G. Hautier, M. Kocher, S. Cholia, D. Gunter, V. L. Chevrier, K. A. Persson, and G. Ceder, "Python materials genomics (pymatgen): A robust, open-source python library for materials analysis," Comput. Mater. Sci. **68**, 314–319 (2013).
[54]H. Wang, L. Zhang, J. Han, and W. E, "DeePMD-kit: A deep learning package for many-body potential energy representation and molecular dynamics," Comput. Phys. Commun. **228**, 178–184 (2018).
[55]P. E. Blöchl, "Projector augmented-wave method," Phys. Rev. B **50**, 17953 (1994).
[56]G. Kresse and J. Furthmüller, "Efficient iterative schemes for *ab initio* total-energy calculations using a plane-wave basis set," Phys. Rev. B **54**, 11169 (1996).
[57]G. Kresse and D. Joubert, "From ultrasoft pseudopotentials to the projector augmented-wave method," Phys. Rev. B **59**, 1758 (1999).
[58]W. Kohn and L. J. Sham, "Self-consistent equations including exchange and correlation effects," Phys. Rev. **140**, A1133–A1138 (1965).
[59]J. P. Perdew, K. Burke, and M. Ernzerhof, "Generalized gradient approximation made simple," Phys. Rev. Lett. **77**, 3865–3868 (1996).
[60]J. P. Perdew, A. Ruzsinszky, G. I. Csonka, O. A. Vydrov, G. E. Scuseria, L. A. Constantin, X. Zhou, and K. Burke, "Restoring the density-gradient expansion for exchange in solids and surfaces," Phys. Rev. Lett. **100**, 136406 (2008).
[61]J. Sun, R. C. Remsing, Y. Zhang, Z. Sun, A. Ruzsinszky, H. Peng, Z. Yang, A. Paul, U. Waghmare, X. Wu *et al.*, "SCAN: An efficient density functional yielding accurate structures and energies of diversely-bonded materials," arXiv:1511.01089 (2015).
[62]J. P. Perdew, M. Ernzerhof, and K. Burke, "Rationale for mixing exact exchange with density functional approximations," J. Chem. Phys. **105**, 9982–9985 (1996).
[63]C. Adamo and V. Barone, "Toward reliable density functional methods without adjustable parameters: The PBE0 model," J. Chem. Phys. **110**, 6158–6170 (1999).
[64]A. Kuhn, V. Duppel, and B. V. Lotsch, "Tetragonal $Li_{10}GeP_2S_{12}$ and Li_7GePS_8–exploring the Li ion dynamics in LGPS Li electrolytes," Energy Environ. Sci. **6**, 3548–3552 (2013).
[65]J. M. Whiteley, J. H. Woo, E. Hu, K.-W. Nam, and S.-H. Lee, "Empowering the lithium metal battery through a silicon-based superionic conductor," J. Electrochem. Soc. **161**, A1812–A1817 (2014).
[66]S. Plimpton, "Fast parallel algorithms for short-range molecular dynamics," J. Comput. Phys. **117**, 1–19 (1995).
[67]D. A. Weber, A. Senyshyn, K. S. Weldert, S. Wenzel, W. Zhang, R. Kaiser, S. Berendts, J. Janek, and W. G. Zeier, "Structural insights and 3D diffusion pathways within the lithium superionic conductor $Li_{10}GeP_2S_{12}$," Chem. Mater. **28**, 5905–5915 (2016).
[68]I.-C. Yeh and G. Hummer, "System-size dependence of diffusion coefficients and viscosities from molecular dynamics simulations with periodic boundary conditions," J. Phys. Chem. B **108**, 15873–15879 (2004).

Published under license by AIP Publishing

[69]J. C. Bachman, S. Muy, A. Grimaud, H.-H. Chang, N. Pour, S. F. Lux, O. Paschos, F. Maglia, S. Lupart, P. Lamp, L. Giordano, and Y. Shao-Horn, "Inorganic solid-state electrolytes for lithium batteries: Mechanisms and properties governing ion conduction," Chem. Rev. **116**, 140–162 (2016).
[70]W. Fitzhugh, L. Ye, and X. Li, "The effects of mechanical constriction on the operation of sulfide based solid-state batteries," J. Mater. Chem. A **7**, 23604–23627 (2019).
[71]S. Ohno, T. Bernges, J. Buchheim, M. Duchardt, A.-K. Hatz, M. A. Kraft, H. Kwak, A. L. Santhosha, Z. Liu, N. Minafra, F. Tsuji, A. Sakuda, R. Schlem, S. Xiong, Z. Zhang, P. Adelhelm, H. Chen, A. Hayashi, Y. S. Jung, B. V. Lotsch, B. Roling, N. M. Vargas-Barbosa, and W. G. Zeier, "How certain are the reported ionic conductivities of thiophosphate-based solid electrolytes? An interlaboratory study," ACS Energy Lett. **5**, 910–915 (2020).
[72]G. Murch, "The Haven ratio in fast ionic conductors," Solid State Ionics **7**, 177–198 (1982).
[73]A. P. Bartók, R. Kondor, and G. Csányi, "On representing chemical environments," Phys. Rev. B **87**, 184115 (2013).
[74]N. Bernstein, B. Bhattarai, G. Csányi, D. A. Drabold, S. R. Elliott, and V. L. Deringer, "Quantifying chemical structure and machine-learned atomic energies in amorphous and liquid silicon," Angew. Chem. **131**, 7131–7135 (2019).
[75]Y. Kato, S. Hori, T. Saito, K. Suzuki, M. Hirayama, A. Mitsui, M. Yonemura, H. Iba, and R. Kanno, "High-power all-solid-state batteries using sulfide superionic conductors," Nat. Energy **1**, 16030 (2016).
[76]T. Xie, A. France-Lanord, Y. Wang, Y. Shao-Horn, and J. C. Grossman, "Graph dynamical networks for unsupervised learning of atomic scale dynamics in materials," Nat. Commun. **10**, 2667 (2019).
[77]Y. Deng, C. Eames, J.-N. Chotard, F. Lalère, V. Seznec, S. Emge, O. Pecher, C. P. Grey, C. Masquelier, and M. S. Islam, "Structural and mechanistic insights into fast lithium-ion conduction in Li_4SiO_4–Li_3PO_4 solid electrolytes," J. Am. Chem. Soc. **137**, 9136–9145 (2015).
[78]L. Kahle, A. Musaelian, N. Marzari, and B. Kozinsky, "Unsupervised landmark analysis for jump detection in molecular dynamics simulations," Phys. Rev. Mater. **3**, 055404 (2019).
[79]S. Muy, J. C. Bachman, H.-H. Chang, L. Giordano, F. Maglia, S. Lupart, P. Lamp, W. G. Zeier, and Y. Shao-Horn, "Lithium conductivity and Meyer-Neldel rule in Li_3PO_4–Li_3VO_4–Li_4GeO_4 lithium superionic conductors," Chem. Mater. **30**, 5573–5582 (2018).
[80]R. P. Rao, N. Sharma, V. K. Peterson, and S. Adams, "Formation and conductivity studies of lithium argyrodite solid electrolytes using *in-situ* neutron diffraction," Solid State Ionics **230**, 72–76 (2013).
[81]D. P. Kingma and J. Ba, "Adam: A method for stochastic optimization," arXiv:1412.6980 (2014).
[82]L. Zhang, J. Han, H. Wang, R. Car, and W. E, "Deep potential molecular dynamics: A scalable model with the accuracy of quantum mechanics," Phys. Rev. Lett. **120**, 143001 (2018).
[83]S. Hori, S. Taminato, K. Suzuki, M. Hirayama, Y. Kato, and R. Kanno, "Structure–property relationships in lithium superionic conductors having a $Li_{10}GeP_2S_{12}$ -type structure," Acta Crystallogr., Sect. B: Struct. Sci., Cryst. Eng. Mater. **71**, 727–736 (2015).
[84]S. Hori, M. Kato, K. Suzuki, M. Hirayama, Y. Kato, and R. Kanno, "Phase diagram of the Li_4GeS4-Li_3PS_4 quasi-binary system containing the superionic conductor $Li_{10}GeP_2S_{12}$," J. Am. Ceram. Soc. **98**, 3352–3360 (2015).
[85]C. H. Hu, Z. Q. Wang, Z. Y. Sun, and C. Y. Ouyang, "Insights into structural stability and Li superionic conductivity of $Li_{10}GeP_2S_{12}$ from first-principles calculations," Chem. Phys. Lett. **591**, 16–20 (2014).
[86]X. Liang, L. Wang, Y. Jiang, J. Wang, H. Luo, C. Liu, and J. Feng, "In-channel and in-plane Li ion diffusions in the superionic conductor $Li_{10}GeP_2S_{12}$ probed by solid-state NMR," Chem. Mater. **27**, 5503–5510 (2015).
[87]J. P. Perdew, S. Kurth, A. c. v. Zupan, and P. Blaha, "Accurate density functional with correct formal properties: A step beyond the generalized gradient approximation," Phys. Rev. Lett. **82**, 2544–2547 (1999).
[88]A. Kuhn, O. Gerbig, C. Zhu, F. Falkenberg, J. Maier, and B. V. Lotsch, "A new ultrafast superionic Li-conductor: Ion dynamics in $Li_{11}Si_2PS_{12}$ and comparison with other tetragonal LGPS-type electrolytes," Phys. Chem. Chem. Phys. **16**, 14669–14674 (2014).
[89]Z. Q. Wang, M. S. Wu, G. Liu, X. L. Lei, B. Xu, and C. Y. Ouyang, "Elastic properties of new solid state electrolyte material $Li_{10}GeP_2S_{12}$: A study from first-principles calculations," Int. J. Electrochem. Sci. **9**, 562–568 (2014); available at http://www.electrochemsci.org/list14.htm.
[90]J. Klimeš, D. R. Bowler, and A. Michaelides, "Chemical accuracy for the van der Waals density functional," J. Phys.: Condens. Matter **22**, 022201 (2009).
[91]S. Hori, K. Suzuki, M. Hirayama, Y. Kato, T. Saito, M. Yonemura, and R. Kanno, "Synthesis, structure, and ionic conductivity of solid solution, $Li_{10+\delta}M_{1+\delta}P_{2-\delta}S_{12}$ (M = Si, Sn)," Faraday Discuss. **176**, 83–94 (2015).

Published under license by AIP Publishing